

Science  
**Signaling**

24 June 2014

 AAAS

---

The following resources related to this article are available online at <http://stke.sciencemag.org>.  
This information is current as of 25 June 2014.

---

- Article Tools** Visit the online version of this article to access the personalization and article tools:  
<http://stke.sciencemag.org/cgi/content/full/sigtrans;7/331/ra59>
- Supplemental Materials** "Supplementary Materials"  
<http://stke.sciencemag.org/cgi/content/full/sigtrans;7/331/ra59/DC1>
- References** This article cites 43 articles, 15 of which can be accessed for free:  
<http://stke.sciencemag.org/cgi/content/full/sigtrans;7/331/ra59#otherarticles>
- Glossary** Look up definitions for abbreviations and terms found in this article:  
<http://stke.sciencemag.org/glossary/>
- Permissions** Obtain information about reproducing this article:  
<http://www.sciencemag.org/about/permissions.dtl>

# Reliable Encoding of Stimulus Intensities Within Random Sequences of Intracellular Ca<sup>2+</sup> Spikes

Kevin Thurley,<sup>1,2,3</sup> Stephen C. Tovey,<sup>2</sup> Gregor Moenke,<sup>1</sup> Victoria L. Prince,<sup>4</sup> Abha Meena,<sup>2</sup> Andrew P. Thomas,<sup>4</sup> Alexander Skupin,<sup>5,6</sup> Colin W. Taylor,<sup>2\*</sup> Martin Falcke<sup>1,7\*</sup>

Ca<sup>2+</sup> is a ubiquitous intracellular messenger that regulates diverse cellular activities. Extracellular stimuli often evoke sequences of intracellular Ca<sup>2+</sup> spikes, and spike frequency may encode stimulus intensity. However, the timing of spikes within a cell is random because each interspike interval has a large stochastic component. In human embryonic kidney (HEK) 293 cells and rat primary hepatocytes, we found that the average interspike interval also varied between individual cells. To evaluate how individual cells reliably encoded stimuli when Ca<sup>2+</sup> spikes exhibited such unpredictability, we combined Ca<sup>2+</sup> imaging of single cells with mathematical analyses of the Ca<sup>2+</sup> spikes evoked by receptors that stimulate formation of inositol 1,4,5-trisphosphate (IP<sub>3</sub>). This analysis revealed that signal-to-noise ratios were improved by slow recovery from feedback inhibition of Ca<sup>2+</sup> spiking operating at the whole-cell level and that they were robust against perturbations of the signaling pathway. Despite variability in the frequency of Ca<sup>2+</sup> spikes between cells, steps in stimulus intensity caused the stochastic period of the interspike interval to change by the same factor in all cells. These fold changes reliably encoded changes in stimulus intensity, and they resulted in an exponential dependence of average interspike interval on stimulation strength. We conclude that Ca<sup>2+</sup> spikes enable reliable signaling in a cell population despite randomness and cell-to-cell variability, because global feedback reduces noise, and changes in stimulus intensity are represented by fold changes in the stochastic period of the interspike interval.

## INTRODUCTION

Signaling from receptors in the plasma membrane requires a strong correlation between the extracellular stimulus and downstream intracellular events if information is not to be lost. The mechanisms by which changes in extracellular stimulus intensity are reliably converted into graded changes in cellular activity have not been fully resolved. It is unclear, for example, whether individual cells reliably transmit changes in the intensity of an extracellular stimulus to a graded change in cellular activity or whether the correlation between stimulus intensity and cellular response is realized largely by the average behavior of many cells (*1*). The complex spatiotemporal organization of the changes in cytosolic free Ca<sup>2+</sup> concentration ([Ca<sup>2+</sup>]<sub>i</sub>) evoked by receptors that stimulate formation of inositol 1,4,5-trisphosphate (IP<sub>3</sub>) enables Ca<sup>2+</sup> to regulate many cellular events (*2–8*). IP<sub>3</sub> receptors (IP<sub>3</sub>Rs) are intracellular Ca<sup>2+</sup> channels located on the endoplasmic reticulum (ER). Opening of IP<sub>3</sub>Rs is stimulated by IP<sub>3</sub> and Ca<sup>2+</sup> (*9*), allowing them to propagate Ca<sup>2+</sup> signals regeneratively. As IP<sub>3</sub> concentrations increase, openings of single IP<sub>3</sub>Rs lead to coordinated opening of clustered IP<sub>3</sub>Rs, and then to cytosolic Ca<sup>2+</sup> waves (*10*). Repetitive initiation of these waves generates sequences of Ca<sup>2+</sup> spikes, the frequency of which often increases with stimulus intensity (*2, 11, 12*). This repetitive spiking behavior is not limited to Ca<sup>2+</sup> signaling because there are examples of other signaling pathways

in which sustained stimuli evoke pulsatile intracellular signals or responses (*13, 14*). The location, amplitude, duration, and frequency of Ca<sup>2+</sup> signals are likely to convey information (*2–8, 12*). However, most supporting evidence comes from biochemical analyses (*6*), experimentally imposed Ca<sup>2+</sup> spikes (*4, 6*), or analysis of cell populations (*4*). Few examples directly demonstrate that individual cells can mount graded responses to changes in extracellular stimulus intensity by decoding Ca<sup>2+</sup> spikes (*5, 7, 8*).

In various cells, extracellular stimuli evoke trains of Ca<sup>2+</sup> spikes for which the interspike intervals (ISIs) are not predictable, because each ISI has a large random component (*15*). Thus, we investigated whether there are features of the relationship between stimulus and ISI that enabled reliable encoding of stimulus intensity in the spike frequency. We analyzed Ca<sup>2+</sup> spikes by imaging single cells exposed to ligands that stimulate IP<sub>3</sub>-evoked Ca<sup>2+</sup> signals. We then performed mathematical analysis to identify properties of the sequences of spikes that correlated with stimulus intensity, and tested those properties for robustness against variability between cells.

## RESULTS

### Ca<sup>2+</sup> spike sequences exhibit temporal randomness and large cell-to-cell variability

We performed Ca<sup>2+</sup> imaging of individual cells exposed to ligands that activate phospholipase C (PLC) through G protein (heterotrimeric guanine nucleotide-binding protein)-coupled receptors (GPCRs), thereby stimulating production of IP<sub>3</sub> and Ca<sup>2+</sup> release from the ER (Fig. 1A). We imaged human embryonic kidney (HEK) 293 cells exposed to carbachol (CCh), an agonist of muscarinic acetylcholine receptors, or rat primary hepatocytes exposed to either vasopressin or phenylephrine, an agonist of α<sub>1</sub>-adrenoceptors (Fig. 1B, upper). We measured the ISI for sequences of spikes occurring in individual cells (Fig. 1B, middle), and plotted the average ISI ( $T_{av}$ ) and its SD ( $\sigma$ ) for each condition (Fig. 1B, bottom) (abbreviations and symbols are listed in table S1).

<sup>1</sup>Mathematical Cell Physiology, Max Delbrück Center for Molecular Medicine, Robert Rössle Straße 10, Berlin 13125, Germany. <sup>2</sup>Department of Pharmacology, University of Cambridge, Tennis Court Road, Cambridge CB2 1PD, UK. <sup>3</sup>Institute for Theoretical Biology, Charité-Universitätsmedizin Berlin, Invalidenstraße 43, Berlin 10115, Germany. <sup>4</sup>Department of Pharmacology and Physiology, New Jersey Medical School, Rutgers, The State University of New Jersey, 185 South Orange Avenue, Newark, NJ 07103, USA. <sup>5</sup>Luxembourg Centre for Systems Biomedicine, 7 Avenue des Hauts Fourmeaux, Esch sur Alzette 4362, Luxembourg. <sup>6</sup>National Center for Microscopy and Imaging Research, University of California, San Diego, 9500 Gilman Drive, La Jolla, CA 92093, USA. <sup>7</sup>Department of Physics, Humboldt University Berlin, Newtonstraße 15, Berlin 12489, Germany.

\*Corresponding authors. E-mail: martin.falcke@mmdc-berlin.de (M.F.); cwt1000@cam.ac.uk (C.W.T.)

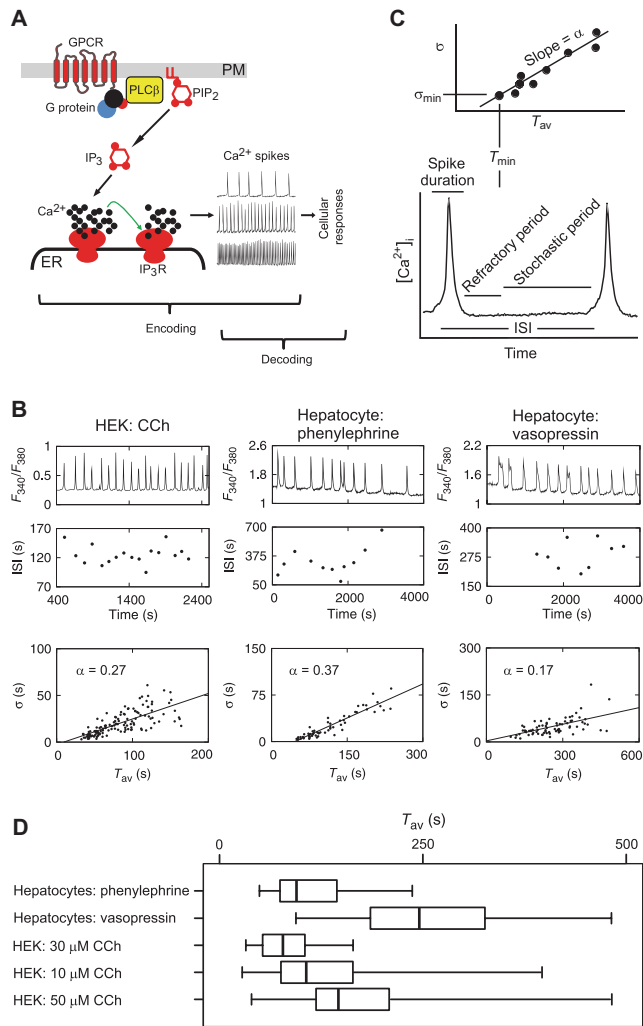


**Fig. 1. Ca<sup>2+</sup> spikes are stochastic and vary between cells.** (A) Many extracellular signals activate GPCRs coupled to G<sub>αq</sub> proteins, which stimulate PLCβ and the production of IP<sub>3</sub>. Binding of IP<sub>3</sub> and Ca<sup>2+</sup> to IP<sub>3</sub>R triggers release of Ca<sup>2+</sup> into the cytosol. The increase in [Ca<sup>2+</sup>]<sub>i</sub> can then activate neighboring IP<sub>3</sub>R to generate a Ca<sup>2+</sup> wave. Repetitive initiation of Ca<sup>2+</sup> waves generates sequences of Ca<sup>2+</sup> spikes that vary in frequency. Information is encoded in the properties of these spike sequences and decoded by downstream effectors. PM, plasma membrane. (B) Ca<sup>2+</sup> signals in HEK293 cells and hepatocytes. HEK293 cells were stimulated with CCh (30 μM), and hepatocytes with phenylephrine (1 μM) or vasopressin (10 nM). Top: [Ca<sup>2+</sup>]<sub>i</sub> is shown for typical cells as fura-2 fluorescence ratios (F<sub>340</sub>/F<sub>380</sub>). Middle: Individual ISIs from the traces above. Bottom: For each cell, average ISI (T<sub>av</sub>) and its SD (σ) provide a single point on the T<sub>av</sub>-σ relation. The ratio of axes scales is preserved in the three T<sub>av</sub>-σ plots to allow direct comparison of their slopes. (C) ISI comprises the spike duration and the refractory period (the sum of which is T<sub>min</sub>), and the stochastic period (T<sub>av</sub> - T<sub>min</sub>). T<sub>av</sub> and σ are linearly related with slope α. α<sub>min</sub> is the SD of sequences with T<sub>av</sub> = T<sub>min</sub>. (D) Box plots of T<sub>av</sub> from HEK293 cells stimulated with CCh (10 μM, n = 81; 30 μM, n = 135; or 50 μM, n = 50) or hepatocytes stimulated with phenylephrine (1 μM, n = 60) or vasopressin (10 nM, n = 77). Bold lines indicate medians, boxes show interquartile ranges, and whiskers show minima and maxima. Results from hepatocytes and HEK293 cells stimulated with 30 μM CCh correspond to data shown in (B).

Repetitive Ca<sup>2+</sup> spiking in stimulated HEK293 cells, hepatocytes, and many other cells (2, 11, 12, 16) creates a false impression that Ca<sup>2+</sup> spikes are predictable (15, 17). All biological processes include some variability (18), but we found that in stimulated HEK293 cells and hepatocytes, a distinguishing feature of the Ca<sup>2+</sup> spikes was the correlation between the variability of the ISI within each cell (σ) and T<sub>av</sub>. This relationship between σ and T<sub>av</sub> has been described previously for Ca<sup>2+</sup> spikes in HEK293 cells, astrocytes, microglia, processed lipoaspirate (PLA) cells (15), and endothelial progenitor cells (17). The correlation is captured in the T<sub>av</sub>-σ relation (Fig. 1B, bottom):

$$\sigma = \alpha(T_{av} - T_{min}) + \sigma_{min} \quad (1)$$

where T<sub>min</sub> is the sum of the spike duration and refractory period, and σ<sub>min</sub> is the SD of ISI sequences with T<sub>av</sub> = T<sub>min</sub>. The ISI has three components (Fig. 1C): spike duration, refractory period, and an interval before the next spike initiates that terminates stochastically (15). For Ca<sup>2+</sup> spikes, the relationship between T<sub>av</sub> and σ reveals the contribution of such a stochastic process to the ISI. This stochastic period shortens as the stimulus intensity increases until it becomes so brief that a spike initiates almost as soon as a cell emerges from the refractory period (15). With high stimulus intensities, spike sequences would have an average ISI equal to T<sub>min</sub>, and the ISIs would become almost uniform, with a small σ (σ<sub>min</sub>). Under all other conditions, the stochastic component makes a major contribution to the ISI.

We observed that there is also variability in T<sub>av</sub> between cells treated with the same stimulus (Fig. 1D). Under various conditions, this variability between cells often exceeded T<sub>av</sub> for the cell population, indicating that there is no consistent relationship between stimulus intensity and T<sub>av</sub> that applies to all cells. These data indicated that there are at least two potential impediments to transferring information reliably from extracellular signals through repetitive Ca<sup>2+</sup> spikes: individual cells differ in their sensitivities to stimuli, and within cells, Ca<sup>2+</sup> spike sequences have a stochastic or random component.

### The signal-to-noise ratio is increased by negative feedback and robust against cell-to-cell variability

The ISI comprises fixed components (T<sub>min</sub>: the spike duration and the refractory period) and a stochastic period (Fig. 1C, bottom). By analyzing the temporal randomness of the ISI, we can determine how the probability of a spike occurring changes with time after the refractory period. Therefore, we examined many sequences of stimulus-evoked Ca<sup>2+</sup> spikes to determine the variability of the ISI. If the probability of a spike occurring stepped immediately to its final value, the occurrence of each spike would be unaffected by the timing of any preceding Ca<sup>2+</sup> spike. The slope of the T<sub>av</sub>-σ relation (α) would then be 1 (15), that is, the ISIs would be described by a Poisson distribution. Once the refractory period had passed, the timing of the next Ca<sup>2+</sup> spike would then behave like the random decay of radioactive atoms. Under this condition, the signal-to-noise ratio (α<sup>-1</sup>), and thus the information content of the signal, would have their minimal values (19, 20). There is, however, an interval after the refractory period when the cell recovers from negative feedback inhibition toward the maximal probability of firing another Ca<sup>2+</sup> spike (eq. S4, fig. S1, and text S1: Mathematical description of ISI distributions) (15, 17, 19). This lingering inhibition after the refractory period delays the time at which the information content of the signal becomes minimal. The time scale of recovery from feedback inhibition is, therefore, critical in determining the reliability of signaling: slow recovery from feedback inhibition improves reliability by increasing signal-to-noise ratios (reducing α) (eqs. S3 and S6, fig. S2, and text S1: Mathematical description of ISI distributions) (21, 22).

For hepatocytes and HEK293 cells,  $\alpha$  is less than 1 (Fig. 1B), indicating the involvement of feedback inhibition with a recovery time after the refractory period that is at least as long as the ISI (23). Because the ISI can range from tens of seconds to several minutes, the recovery is too slow to result from known properties of clustered IP<sub>3</sub>Rs: the intervals between Ca<sup>2+</sup> signals evoked by clusters of IP<sub>3</sub>Rs, often described as Ca<sup>2+</sup> puffs, are no more than a few seconds (23). The feedback inhibition must, therefore, be “global,” that is, a consequence of the Ca<sup>2+</sup> spike invading the entire cell, rather than the result of local Ca<sup>2+</sup> signaling from clusters of IP<sub>3</sub>Rs. Such global mechanisms could include regulation of IP<sub>3</sub> metabolism (12), changes in the sensitivity of IP<sub>3</sub>Rs to IP<sub>3</sub> or Ca<sup>2+</sup> (9), or store depletion. The value of  $\alpha$  is different for HEK293 cells and hepatocytes, and different for hepatocytes stimulated with different stimuli (Fig. 1B). That different stimuli produced different values of  $\alpha$  suggested that the slowly reversing feedback mechanism must regulate signaling events specifically associated with GPCRs.

Because a high signal-to-noise ratio is advantageous, we examined how the ratio was affected by perturbations of steps within the Ca<sup>2+</sup> signaling pathway. Theoretical analyses predict that  $\alpha$  should be unaffected by such perturbations unless they affect the global feedback mechanism (21, 24), the molecular targets of which have not yet been identified (12). Thus, changes in PLC activity, for example, would not be expected to affect  $\alpha$  unless PLC contributed to the global feedback. Conversely, changing the Ca<sup>2+</sup> sensitivity of a sensor mediating the feedback by, for example, altering the activity of IP<sub>3</sub> 3-kinase, a kinase that inactivates IP<sub>3</sub> (25), or influencing coupling of the GPCR to G proteins and downstream signaling events would affect  $\alpha$ . Because the theoretical predictions have not been investigated experimentally, we perturbed various steps in the GPCR-mediated Ca<sup>2+</sup> signaling pathway to determine their effects on ISI. We then calculated  $\alpha$  to determine the consequences of the perturbations on the signal-to-noise ratio.

In the HEK293 cells, CCh activates muscarinic acetylcholine receptors coupled to G $\alpha_q$ , which stimulate PLC and thus IP<sub>3</sub>-mediated Ca<sup>2+</sup> release from the ER. In the same cells, a stably expressed receptor for human parathyroid hormone (PTH) couples to G $\alpha_s$ , which stimulates adenylyl cyclase to promote accumulation of adenosine 3',5'-monophosphate (cAMP). cAMP directly increases the sensitivity of IP<sub>3</sub>Rs to IP<sub>3</sub> (26). We analyzed the ISI of spikes triggered by CCh in the presence or absence of U73122 to inhibit PLC (27), PTH to increase IP<sub>3</sub>R sensitivity (26), or cyclopiazonic acid (CPA) to inhibit the sarcolemmal/endoplasmic reticulum Ca<sup>2+</sup>-ATPase (SERCA) (28) that pumps Ca<sup>2+</sup> into the ER (Fig. 2A). Ca<sup>2+</sup> imaging analysis showed that these manipulations changed the frequency of CCh-evoked Ca<sup>2+</sup> spikes: PTH increased their frequency (shortened  $T_{av}$ ), whereas U73122 and CPA decreased Ca<sup>2+</sup> spike frequency (increased  $T_{av}$ ) (Fig. 2, B and C, and fig. S3A). Despite substantial changes in  $T_{av}$ , none of these perturbations changed  $\alpha$  (Fig. 2, D and E). Varying the concentration of CCh also changed  $T_{av}$  without affecting  $\alpha$  (fig. S3B). Thus, cells can produce Ca<sup>2+</sup> spikes with a constant signal-to-noise ratio despite perturbations to the signaling pathway that alter the frequency of the spikes. We found that the signal-to-noise ratio is specific for each cell type (Figs. 1B and 2E) and that within hepatocytes, it varies with the stimulus (Fig. 2E). Thus, the downstream mechanisms that decode Ca<sup>2+</sup> spikes receive signals in which the signal-to-noise ratio is defined, and it is robust to variations within the pathway that trigger the spikes.

### Stimulation steps are encoded by fold changes in the average stochastic period of the ISI

We found that Ca<sup>2+</sup> spikes in two different cell types responding to three different extracellular stimuli exhibited a stochastic component in the ISI (Figs. 1B and 2D), and  $T_{av}$  for cells exposed to identical stimuli varied widely between individual cells (Fig. 1D). With this amount of variability, how might Ca<sup>2+</sup> spikes encode extracellular stimulus intensities?

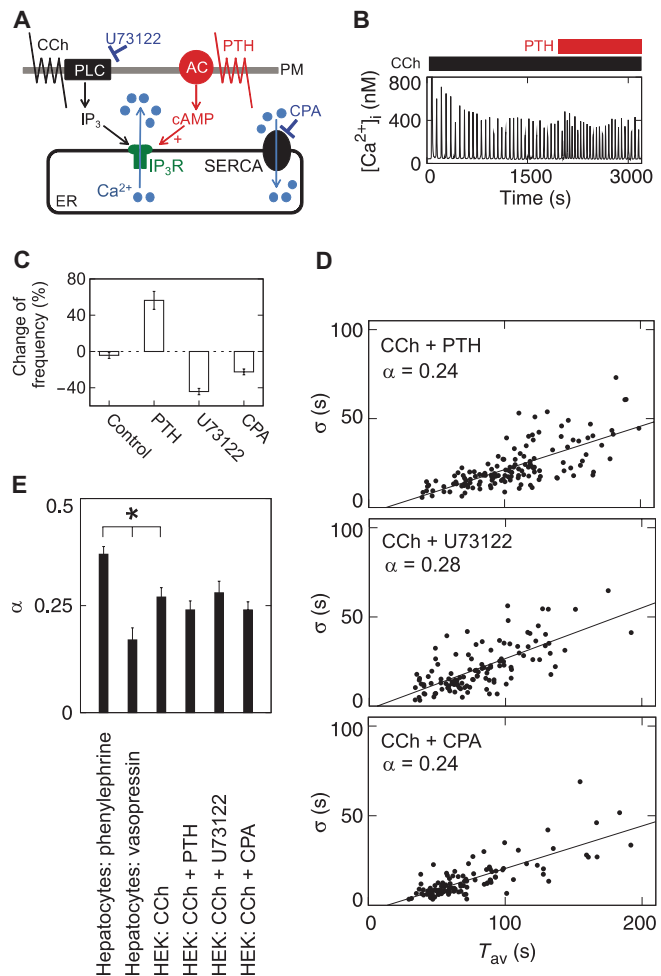


**Fig. 2. Robust signal-to-noise ratios of stochastic Ca<sup>2+</sup> signals.** (A) Diagram of the pathway that stimulates Ca<sup>2+</sup> spikes in HEK293 cells and the perturbations tested. CCh stimulates PLC producing IP<sub>3</sub> that releases Ca<sup>2+</sup> from ER through IP<sub>3</sub>Rs. U73122 inhibits PLC. PTH stimulates adenylyl cyclase (AC) and formation of cAMP, which increases IP<sub>3</sub>R sensitivity. Cyclopiazonic acid (CPA) reversibly inhibits the sarco/endoplasmic reticulum Ca<sup>2+</sup>-ATPase (SERCA). (B) [Ca<sup>2+</sup>]<sub>i</sub> in a HEK293 cell exposed to two sequential stimuli. In this representative experiment, PTH was added to cells in the continued presence of CCh. The presence of CCh (30 μM) and PTH (100 nM) is indicated by the black and red bars, respectively. (C) Change in Ca<sup>2+</sup> spike frequency ( $1/T_{av}$ ) in HEK293 cells after a perturbation of the signaling pathway. The experiments were performed similarly to the experiment shown in (B), but with two successive challenges with CCh alone (30 μM) (control, 21 cells), or CCh alone followed by CCh with PTH (100 nM, 31 cells), U73122 (100 nM, 35 cells), or CPA (10 nM, 33 cells) (see fig. S3A for the responses recorded from each cell). Results (means ± SEM) show the change in Ca<sup>2+</sup> spike frequency ( $1/T_{av2} - 1/T_{av1}$ ) between successive challenges as a percentage of the first frequency ( $1/T_{av1}$ ). CPA had no effect on [Ca<sup>2+</sup>]<sub>i</sub> in unstimulated cells ( $62 \pm 16$  nM and  $58 \pm 6$  nM, mean ± SEM, before and 10 min after CPA addition;  $n = 48$  cells). For all, except the successive CCh stimuli (control), the change in spike frequency was significant ( $P < 0.05$ , Student's *t* test). (D)  $T_{av}$ - $\sigma$  relations for HEK293 cells stimulated with CCh in the presence of PTH, U73122, or CPA at the concentrations described in (C). (E) Slopes of the  $T_{av}$ - $\sigma$  relation ( $\alpha \pm 95\%$  confidence intervals) in hepatocytes or HEK293 cells exposed to the conditions indicated (\* $P < 0.05$ , *F*-test).

In sensory perception, Weber’s law proposes that the ability to detect a small change in stimulus is a constant fraction of the initial stimulus (29). Therefore, we evaluated whether fold changes in the stochastic period of the ISI might encode stimulus intensities in a way that was insensitive to the variability between cells. Such fold changes in ISI would more reliably encode stimulus intensities than absolute values only if the fold changes were less variable than the absolute values. As a starting point, we define the fold change ( $\beta$ ) as the change of the stochastic period relative to its initial value:

$$\frac{(T_{av1} - T_{min}) - (T_{av2} - T_{min})}{T_{av1} - T_{min}} = \beta \quad (2)$$

where  $T_{av1}$  and  $T_{av2}$  are average ISIs with different stimulus intensities, and  $T_{min}$  is the same as in Eq. 1. (see Fig. 1C and table S1). Equation 2 implies a linear relationship between  $\Delta T_{av} = T_{av1} - T_{av2}$  and  $T_{av1} - T_{min}$ . The linear relationship is also predicted by an independently derived stochastic model, which is illustrated in Fig. 3A, and includes only basic properties of IP<sub>3</sub>R clusters (21) (see Materials and Methods). We refer to this relationship between the change of the stochastic period ( $\Delta T_{av}$ ) relative to its initial value as the “encoding relation,” because as we show later,  $\beta$  reliably encodes changes in stimulus intensity:

$$\Delta T_{av} = \beta(T_{av1} - T_{min}) \quad (3)$$

We tested whether this relation (Eq. 3) applies to Ca<sup>2+</sup> spiking using a paired stimulation protocol in which we stimulated HEK293 cells with one concentration of CCh and then switched the medium to one with a higher concentration (Fig. 3B). The amplitude of the Ca<sup>2+</sup> spikes remained similar when the concentration of CCh was increased: for the largest step (30 to 200  $\mu$ M CCh), the peak amplitude was  $154 \pm 21$  nM ( $n = 23$  cells, 292 spikes) for the first stimulation, and  $155 \pm 18$  nM (632 spikes) for the second. Changes in stimulus intensity are not, therefore, encoded by spike amplitudes. Instead,  $T_{av}$  changed with stimulus intensity in accord with Eq. 3, and the stimulation step affected  $\beta$ , where  $\beta$  is the slope of the lines (Fig. 3C and table S2). The smallest step in CCh concentration (from 50  $\mu$ M to 100  $\mu$ M) caused only small changes in  $T_{av}$  (Fig. 3C right, red line). The practicable duration of experiments limits the reliability with which we can measure such small  $\Delta T_{av}$ , because the length of the spike sequences sets the precision with which we can determine  $T_{av}$ . Thus, the linearity of the relationship between  $\Delta T_{av}$  and  $T_{av1} - T_{min}$  was less clear for this small stimulation step than for larger steps. Nevertheless, even with such small changes in stimulus intensity,  $\beta$  increased with the size of the concentration step (Fig. 3C right, table S2), and the value of  $\beta$  obtained fits

well in the context of the additional concentration-response data (Figs. 3H and 4A). Analysis of hepatocytes sequentially stimulated with 0.6  $\mu$ M and then 1  $\mu$ M phenylephrine showed a similar linear relationship between  $\Delta T_{av}$  and  $T_{av1} - T_{min}$  (Fig. 3D). We assessed the linearity of the relationship between  $\Delta T_{av}$  and  $T_{av1} - T_{min}$  using Pearson’s correlation coefficient ( $\rho$ ) and analysis of explained uncertainty ( $u_{ex}$ ) (see Materials and Methods) (30). A value of 1 for  $\rho$  or  $u_{ex}$  establishes a perfect linear correlation. These analyses (Fig. 3E) confirmed that the relation between  $T_{av1} - T_{min}$  and  $\Delta T_{av}$  is linear and that  $\beta$  increases with the stimulus step in agreement with our theoretical predictions (Fig. 3A).

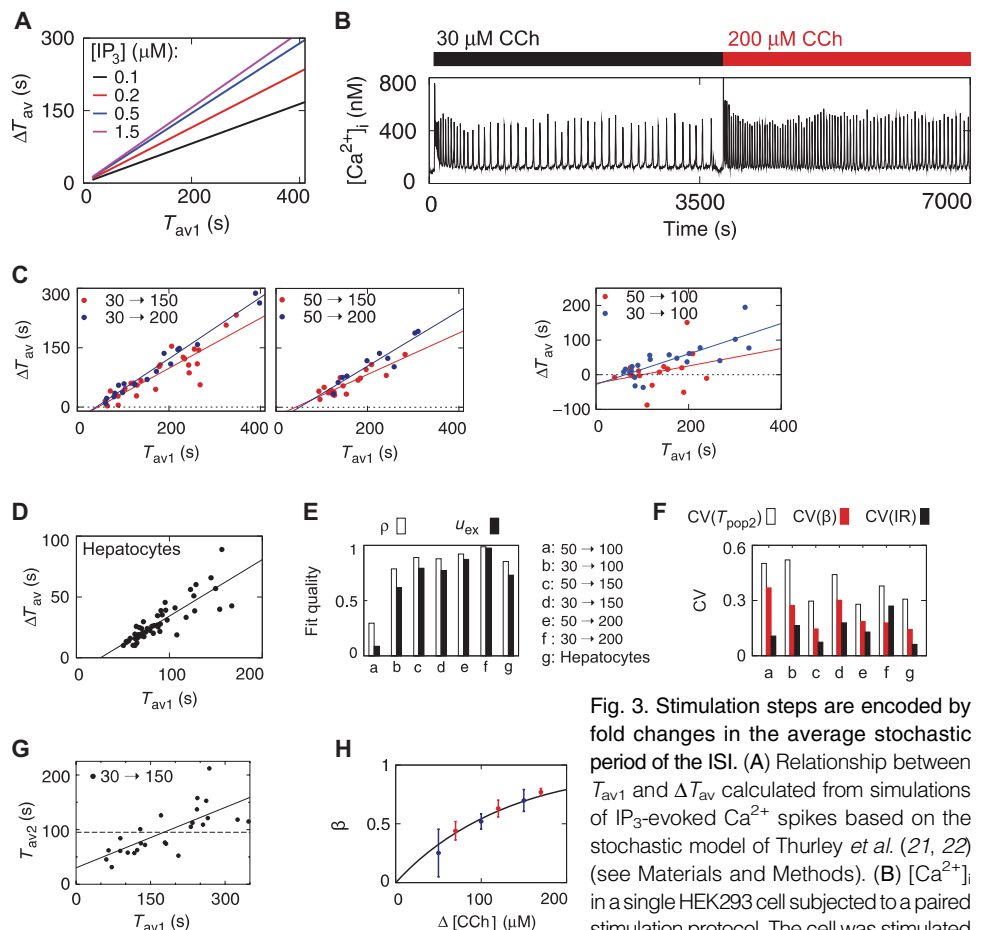


**Fig. 3. Stimulation steps are encoded by fold changes in the average stochastic period of the ISI.** (A) Relationship between  $T_{av1}$  and  $\Delta T_{av}$  calculated from simulations of IP<sub>3</sub>-evoked Ca<sup>2+</sup> spiking based on the stochastic model of Thurley *et al.* (21, 22) (see Materials and Methods). (B) [Ca<sup>2+</sup>]<sub>i</sub> in a single HEK293 cell subjected to a paired stimulation protocol. The cell was stimulated as shown with 30  $\mu$ M CCh before its removal and replacement with 200  $\mu$ M CCh. (C) Relationship between  $T_{av1}$  and  $\Delta T_{av}$  for HEK293 cells successively stimulated with the indicated CCh concentrations ( $\mu$ M) in the paired stimulation protocol (see table S2 for spiking behavior of cells included in the analysis). (D) Relationship between  $T_{av1}$  and  $\Delta T_{av}$  for hepatocytes stimulated with 0.6  $\mu$ M and then 1  $\mu$ M phenylephrine. (E) Pearson’s correlation coefficients ( $\rho$ ) and explained uncertainties ( $u_{ex}$ , Eq. 8) for  $T_{av1}$ - $\Delta T_{av}$  relations for HEK293 cells stimulated with the indicated steps in CCh concentration ( $\mu$ M), or hepatocytes stimulated with 0.6  $\mu$ M and then 1  $\mu$ M phenylephrine. (F) Comparisons of the average deviation of individual cell behavior from  $T_{pop2}$  [ $CV(T_{pop2})$ ] and Eq. 2 [ $CV(\beta)$ ], and the coefficient of variation of the integral ratio [ $CV(IR)$ ] for the paired stimulation protocols. Codes a to g apply to (E) and (F). (G) Relationship between  $T_{av1}$  and  $T_{av2}$  calculated from individual HEK293 cells stimulated first with 30  $\mu$ M and then with 150  $\mu$ M CCh [data from (C)]. The dashed line shows the population average ( $T_{pop2}$ ) of  $T_{av2}$ . The solid line shows Eq. 2 in the form  $T_{av2} = (1 - \beta)T_{av1} + \beta T_{min}$ . (H) Fold changes ( $\beta \pm 95\%$  confidence intervals, Eq. 2) calculated from the slopes of  $T_{av1}$ - $\Delta T_{av}$  relations for all steps in CCh concentration. Symbols are color-coded to indicate the initial CCh concentration (red, 30  $\mu$ M; blue, 50  $\mu$ M). The line shows the exponential relationship between the fold change ( $\beta$ ) and  $\Delta[CCh]$  (Eq. 6), with  $\gamma$  being the only fit parameter,  $\gamma = 7.84 \pm 0.37 \text{ mM}^{-1}$  (mean  $\pm 95\%$  confidence interval).

We assessed whether stimulation steps were more reliably encoded by fold changes ( $\beta$ ) in the average stochastic period of the ISI ( $T_{av} - T_{min}$ ) or by absolute responses ( $T_{av}$ ) by quantifying the variability of each (Fig. 3F), using the data shown in Fig. 3 (C and D). To illustrate the methods used, we describe this analysis for HEK293 cells stimulated first with 30  $\mu$ M and then with 150  $\mu$ M CCh as an example (Fig. 3G). We plotted  $T_{av1}$  and  $T_{av2}$  for each single cell. If absolute responses more reliably encoded the stimulation steps, all values of  $T_{av2}$  should be similar to the population average (that is,  $T_{av2} = T_{pop2}$ , dashed line in Fig. 3G). If fold changes more reliably encoded the stimulation steps, the data should obey Eq. 2, which we rewrite for the purpose of this analysis as  $T_{av2} = (1 - \beta)T_{av1} + \beta T_{min}$  (Fig. 3G, solid line). To determine whether stimulation steps were more reliably encoded by absolute responses or fold changes, we compared the root mean square distances of the data points from these lines. We divided the distance by  $T_{pop2}$  to obtain the coefficient of variation (CV), which can then be compared across the different experiments (a to g) in Fig. 3F (see Materials and Methods, Eqs. 9 and 10). On the basis of this analysis, we found that the relative deviation of  $T_{av2}$  from its population average  $T_{pop2}$  [CV( $T_{pop2}$ ), Eq. 9] was consistently larger than its relative deviation from the encoding relation [CV( $\beta$ ), Eq. 10] (Fig. 3F). Thus, we concluded that  $\beta$  represents individual cell behavior better than does the population average ( $T_{pop}$ ), and  $\beta$  encodes stimulation more reliably than does the average ISI.

Because spike amplitudes and durations were unaffected by stimulus intensity, the integral ratio (IR), that is, the ratio of the area beneath the  $Ca^{2+}$  spikes occurring during the stationary phases of responses to the first stimulus relative to that for the second stimulus, is given by Eq. 11 (see Materials and Methods). To determine whether absolute values or fold changes in the integrated  $Ca^{2+}$  signals more reliably encoded differences in stimulation intensity, we compared the CV( $T_{pop2}$ ) with the CV of the integral ratio CV(IR) for HEK293 cells and hepatocytes stimulated with paired steps in CCh or phenylephrine concentration (Fig. 3F). This comparison showed that fold changes of the integrated  $Ca^{2+}$  signal are less variable than is  $T_{av2}$ . Thus, this analysis indicated that fold changes in the average stochastic period of the ISI and fold changes in the integrated  $Ca^{2+}$  signal more reliably encode stimulus changes than does the average ISI ( $T_{av}$ ).

### Fold changes reliably encode stimulus intensity through an exponential relationship between the stimulus concentration and response

For HEK293 cells exposed to paired steps in CCh concentration, we observed that  $\beta$  depended only on the step size ( $\Delta[CCh]$ ) and not the initial CCh concentration. This is illustrated in Fig. 3H, where the relationship between  $\Delta[CCh]$  and  $\beta$  was the same whether the first challenge was with 30  $\mu$ M (red symbols) or 50  $\mu$ M CCh (blue). We showed in eq. S7 (see text S2: Mathematical derivation of the concentration-response relation) that this observation and Eq. 2 result in the differential equation:

$$\frac{d(T_{av} - T_{min})}{d[CCh]} = -\gamma(T_{av} - T_{min}), \quad \gamma = \frac{\partial\beta}{\partial\Delta[CCh]} \Big|_{\Delta[CCh]=0} \quad (4)$$

The solution to Eq. 4 is the concentration-response relation, which predicts an exponential dependence of  $T_{av}$  on CCh concentration:

$$T_{av} = e^{-\gamma([CCh]-[CCh]_{ref})} (T_{av,ref} - T_{min}) + T_{min} \quad (5)$$

$T_{av,ref}$  is the value of the average ISI measured at a reference CCh concentration ( $[CCh]_{ref}$ ), and  $\gamma$  describes the sensitivity of the stochastic period of  $T_{av}$  to CCh. Cell-to-cell variability appears in Eq. 5 in the variability of  $T_{av,ref}$ , which captures differences between individual cells in the response

of the average stochastic period to CCh. Because Eq. 5 applies to average ISIs, it does not conflict with the randomness of individual ISIs. Inserting Eq. 5 into Eq. 2 shows that these results entail an exponential dependence of  $\beta$  on stimulation step  $\Delta[CCh] = [CCh] - [CCh]_{ref}$ :

$$\beta = 1 - e^{-\gamma\Delta[CCh]} \quad (6)$$

Equation 6 describes the measured data well: The relationship between  $\Delta[CCh]$  and the experimentally determined fold changes ( $\beta$ ) fitted to the exponential function using the fit parameter  $\gamma$  confirmed the reliability with which  $\beta$  describes cell behavior (Fig. 3H).

Analysis of the effects of different CCh concentrations on the population average ( $T_{pop}$ ) of  $T_{av}$ , provided additional support for our suggestion that Eq. 5 appropriately describes the concentration-response relationship. If Eq. 5 correctly describes single-cell behavior, all cells contributing to the population average  $T_{pop}$  must obey the same exponential dependence. Consequently,  $T_{pop}$  is not the sum of exponentials; rather, it obeys a single exponential function:

$$T_{pop} = e^{-\gamma([CCh]-[CCh]_{ref})} (T_{pop,ref} - T_{min}) + T_{min} \quad (7)$$

Therefore, we analyzed the dependence of  $T_{pop}$  derived from analysis of the  $Ca^{2+}$  spikes evoked by different concentrations of CCh in HEK293 cells (Fig. 4A) and found that the relationship was well described by the single exponential function (Eq. 7) with values for  $\gamma$  and  $T_{min}$  obtained from Fig. 3H and Fig. 3C, respectively. This fit of the experimental data to Eq. 7 is inconsistent with  $\beta$  and  $\gamma$  varying substantially between individual cells.

Equation 7 follows from the encoding relation (Eq. 3) and the independence of  $\beta$  from the initial stimulus intensity (Fig. 3H, and see text S2:

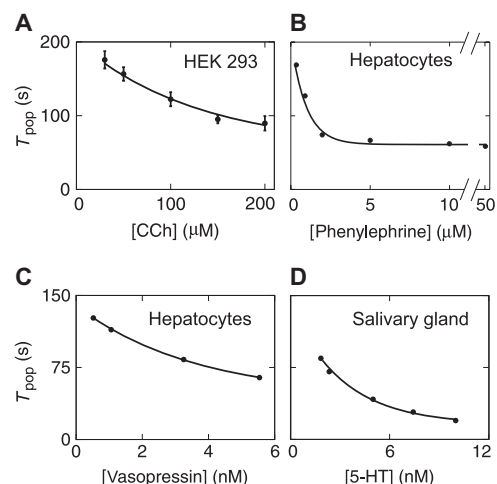


Fig. 4. Fold changes determine a universal concentration-response relation for  $Ca^{2+}$  spikes evoked by stimulation of GPCRs. (A) Population average ( $T_{pop}$ ) of  $T_{av}$  for HEK293 cells at each CCh concentration (means  $\pm$  SEM). Line drawn using the parameter value  $\gamma = 7.84 \text{ mM}^{-1}$  (from the fit to Eq. 6 in Fig. 3H) and  $T_{min} = 57 \text{ s}$  (the average value of  $T_{min}$ s from the six paired-stimulation experiments shown in Fig. 3C), but with no additional curve fitting. (B and C) Relationship between  $T_{pop}$  and ligand concentration for hepatocytes is exponential. Hepatocytes (31) were stimulated with phenylephrine (B) or vasopressin (C). (D) Relationship between  $T_{pop}$  and ligand concentration for insect salivary gland stimulated with 5-HT (32) is exponential. Lines in (B) to (D) are best fits in parameters  $T_{min}$  and  $\gamma$  to Eq. 7: for hepatocytes,  $\gamma = 1.059 \mu\text{M}^{-1}$ ,  $T_{min} = 61 \text{ s}$  (phenylephrine), and  $\gamma = 0.279 \mu\text{M}^{-1}$ ,  $T_{min} = 44 \text{ s}$  (vasopressin); and for salivary gland,  $\gamma = 0.319 \text{ nM}^{-1}$ ,  $T_{min} = 16 \text{ s}$ .

Mathematical derivation of the concentration-response relation). Conversely, if we had started with this exponential concentration-response relationship (Eq. 7) and found that it accurately described the responses of cell populations, it follows that Eqs. 2, 5, and 6 would apply, and that  $\beta$  would be independent of the initial stimulus intensity. To test if Eq. 7 accurately described experimentally determined concentration-response relations, we used our measurements of  $T_{\text{pop}}$  from CCh-stimulated HEK293 cells (Fig. 4A) and published data for hepatocytes (31) and insect salivary glands (32). Data from Rooney *et al.* (31) provided measurements of the frequency of the  $\text{Ca}^{2+}$  spikes evoked by different concentrations of phenylephrine or vasopressin in hepatocytes (Fig. 4, B and C). Data from Rapp and Berridge (32) with blowfly salivary glands provided measurements of the frequency of the  $\text{Ca}^{2+}$ -regulated changes in transepithelial membrane potential evoked by different concentrations of 5-hydroxytryptamine (5-HT) (Fig. 4D). For the published data, we derived  $T_{\text{pop}}$  from the frequency of the spiking responses, and then used least-square nonlinear regression to fit the relationships between stimulus concentration and  $T_{\text{pop}}$  (Fig. 4, B to D), with both  $T_{\text{min}}$  and  $\gamma$  as fitting parameters (the values are provided in the legend of Fig. 4). In each case, the effects of stimulus intensity on  $T_{\text{pop}}$  were well described by Eq. 7: The concentration-response relation was exponential, the response to maximal stimulation was the sum of spike duration and refractory period ( $T_{\text{min}}$ , Fig. 1C), and stimulation controlled the average stochastic period of the ISI ( $T_{\text{av}} - T_{\text{min}}$ ).

## DISCUSSION

All biological systems are variable (18, 33–35). Heterogeneity between cells can have beneficial effects, such as contributing to adaptability (36), increasing the range of sensitivities to extracellular stimuli (1), and providing robustness (37). However, heterogeneity may also distort relationships between stimulus and response. We found that the frequency of  $\text{Ca}^{2+}$  spikes in individual cells varied with stimulus intensity, but that no consistent relationship applied to all cells in the population (Fig. 1D). We identified two general features of receptor-regulated  $\text{Ca}^{2+}$  spiking that enable effective encoding of stimulus intensity.

First,  $\text{Ca}^{2+}$  spikes occurred with a reliable signal-to-noise ratio. Our observation that the slope ( $\alpha$ ) of the  $T_{\text{av}}-\sigma$  relation was constant between cells exposed to the same type of stimulus formed the basis for this conclusion (Fig. 2E and fig. S3B). Furthermore,  $\alpha$  determines the quality of signal transmission (19): A small  $\alpha$  enables more information to be transmitted by spike sequences. We showed that the value of  $\alpha$  was unaffected by stimulus intensity (fig. S3B), as predicted earlier by mathematical modeling (21), nor was  $\alpha$  affected by perturbations of the signaling pathway, like inhibition of PLC, sensitization of  $\text{IP}_3\text{Rs}$ , or inhibition of  $\text{Ca}^{2+}$  uptake by the ER (Fig. 2), that do not affect recovery from global negative feedback. The value of  $\alpha$ , and thus the signal-to-noise ratio, is predicted to depend on the time scale of recovery from global negative feedback (19, 21), which our results suggested is likely to operate close to GPCRs, because  $\alpha$  was different for different extracellular stimuli (Fig. 1E).

Second, changes in extracellular stimulus intensity (ligand concentration) were encoded by fold changes in the average stochastic period of the ISI ( $T_{\text{av}} - T_{\text{min}}$ ), rather than by  $T_{\text{av}}$  itself. The fold change ( $\beta$ ) was similar for each cell, but it varied with stimulus step size, and  $\beta$  correlated better with stimulus intensity than did  $T_{\text{pop}}$  (Fig. 3F). Many effectors, including transcription factors, integrate  $\text{Ca}^{2+}$  signals (1, 3, 17, 38). Fold changes in the stochastic period of the ISI lead to integrated  $\text{Ca}^{2+}$  signals that also occur as approximate fold changes (IR in Fig. 3F). Thus, downstream effectors that respond to integrated  $\text{Ca}^{2+}$  signals will also benefit from the reliability of  $\beta$  (3, 4, 38). Our observation that stimulus intensities are encoded by fold changes in  $\text{Ca}^{2+}$  signals may provide the explanation for downstream cellular activities responding with fold changes (3, 4, 38).

Our findings resulted in a fundamental equation (Eq. 4), which can be applied to all signals that generate a fold change in response. The solution to this equation for  $\text{Ca}^{2+}$  signaling (Eqs. 5 and 7) defines an exponential dependence of  $T_{\text{pop}}$  on stimulus intensity, with individual cells having similar exponents ( $\gamma$ ). Our analysis of three different cell types responding to four different ligands suggested that this relationship is generally applicable to GPCR-stimulated PLC signaling pathways (Fig. 4). Other signaling pathways also exhibit fold changes in responses after stimulation (14): epidermal growth factor-mediated regulation of extracellular signal-regulated kinase 2 (ERK2) has been reported to produce fold changes in the peak of nuclear ERK2 (39), Wnt signaling produces fold changes in the abundance of the transcriptional regulator  $\beta$ -catenin (40), and tumor necrosis factor stimulates fold changes in the nuclear abundance of the transcription factor nuclear factor  $\kappa\text{B}$  (NF- $\kappa\text{B}$ ) (41). We suggest, therefore, that measuring the fold changes according to Eq. 2 for nuclear ERK2,  $\beta$ -catenin, or nuclear NF- $\kappa\text{B}$  and solving the corresponding Eq. 4 would provide the concentration-response relations for these systems (eq. S8).

We determined that, for  $\text{Ca}^{2+}$  spiking, temporal randomness, cell-to-cell variability, and fold changes are unified by an exponential concentration-response relationship that applies to individual cells and the population average (Eqs. 5 and 7). The same features—temporal randomness (42), cell variability (39, 42), and fold changes (39)—have been reported for ERK2 activity, but without a mathematical analysis leading to the concentration-response relation. These analogies between very different signaling systems suggest that we have identified a signaling concept that extends beyond  $\text{Ca}^{2+}$  spiking.

We conclude that despite variability between cells and in the ISIs within cells, there are generic features of  $\text{Ca}^{2+}$  spikes that enable repetitive spikes to encode stimulus intensities. Slow recovery from global feedback provides spike sequences with reliable signal-to-noise ratios. Changes in stimulus intensity are encoded by fold changes ( $\beta$ ) in the average stochastic period of the ISI, which generate exponential concentration-response relationships defined by the stimulus sensitivity ( $\gamma$ ).

## MATERIALS AND METHODS

### Materials

Cell culture media, fura-2 AM, and fluo-4 AM were from Invitrogen. Human PTH (residues 1 to 34) was from Bachem. Other chemicals, including Arg<sup>8</sup>-vasopressin, were from Sigma-Aldrich.

### Single-cell imaging of $[\text{Ca}^{2+}]_i$ in HEK293 cells

HEK293 cells stably transfected with human type 1 PTH receptor (26) were cultured in Dulbecco's modified Eagle's medium/Ham's F-12 supplemented with L-glutamine (2 mM), fetal calf serum (10%), and G-418 (800  $\mu\text{g}/\text{ml}$ ). For imaging experiments, the cells were plated onto 22-mm round glass coverslips coated with 0.01% poly-L-lysine. Cells were loaded with fura-2 AM (2  $\mu\text{M}$ ) for 45 min at 20°C in Hepes-buffered saline (HBS), washed, and imaged after a further 45 min. HBS had the following composition: 135 mM NaCl, 5.9 mM KCl, 1.2 mM  $\text{MgCl}_2$ , 1.5 mM  $\text{CaCl}_2$ , 11.6 mM Hepes, 11.5 mM glucose, pH 7.3. Single-cell fluorescence measurements were performed at 20°C in HBS as previously described (26). Fura-2 fluorescence ratios were collected at 5-s intervals and calibrated to  $[\text{Ca}^{2+}]_i$  after correction for background fluorescence determined after addition of  $\text{MnCl}_2$  (1 mM) and ionomycin (1  $\mu\text{M}$ ) to quench fura-2 fluorescence.

### Single-cell imaging of $[\text{Ca}^{2+}]_i$ in hepatocytes

Hepatocytes were isolated by collagenase perfusion of livers from adult male Sprague-Dawley rats and used on the same day for  $\text{Ca}^{2+}$  imaging

measurements (5, 31). Cells were plated on poly-L-lysine-coated coverslips for 30 min in HBS solution (HBSS). HBSS comprised 121 mM NaCl, 5 mM NaHCO<sub>3</sub>, 4.7 mM KCl, 1.2 mM KH<sub>2</sub>PO<sub>4</sub>, 2 mM CaCl<sub>2</sub>, 1.2 mM MgSO<sub>4</sub>, 10 mM glucose, 100 μM sulfobromophthalein, 0.25% (w/v) fatty acid-free bovine serum albumin, 25 mM Hepes, pH 7.4, at 37°C. Cells were loaded with fura-2 AM (8 μM) for 30 min in the presence of 0.02% (v/v) Pluronic F-127 and immediately transferred to an imaging chamber at 37°C. Pairs of fura-2 fluorescence images using excitation at 340 and 380 nm were collected at 3-s intervals with a cooled charge-coupled device camera and corrected for background fluorescence by release of cytosolic fura-2 using digitonin (25 μg/ml) before calculation of fluorescence ratios for individual cells.

### Analysis of Ca<sup>2+</sup> spikes

In some sequences of Ca<sup>2+</sup> spikes, the stationary phase was preceded by an initial transient in the ISI (see Fig. 3B for an example). Only the stationary components of spike sequences were used for analyses of ISI. In some recordings, there was a linear trend through the entire ISI sequence (see top panels of Fig. 1B). Such a trend, which may reflect slow changes in cellular sensitivity, is not the result of a stochastic process, but it would exaggerate the randomness of ISIs (increase σ) if it were not removed. Therefore, when calculating σ, these trends were removed by subtracting a linear fit to the trend. All other analyses (for example, calculation of T<sub>av</sub>) were performed without this correction.

After normalization using a running average, spikes were identified as an increase in F<sub>340</sub>/F<sub>380</sub> fluorescence of at least 20% from the basal fluorescence ratio. Because long stationary sequences are required to determine σ reliably, only cells in which at least 12 spikes were recorded were used to determine T<sub>av</sub>-σ relations. Within the text, T<sub>av</sub> refers to the average ISI recorded from a single cell (SD, σ), and T<sub>pop</sub> is the average of the T<sub>av</sub>s from a population of identically stimulated cells (see table S1 for definitions and abbreviations). Where only averages of ISIs were analyzed, stationary trains with fewer Ca<sup>2+</sup> spikes (>7) were accepted. Table S2 summarizes the properties of the data used.

Paired Student's *t* tests were used to compare T<sub>av</sub> values from cells exposed to sequential stimuli. *F* tests were used to compare the slopes of T<sub>av</sub>-σ relations. Statistical tests used Prism (version 5, GraphPad Software); *P* < 0.05 was considered significant.

### Calculation of the encoding relation

The building blocks of intracellular Ca<sup>2+</sup> signals are Ca<sup>2+</sup> puffs. These are brief, local increases in [Ca<sup>2+</sup>]<sub>i</sub> that result from the coordinated opening of a few clustered IP<sub>3</sub>Rs (43). Ca<sup>2+</sup> spikes occur when the probability of initiating a Ca<sup>2+</sup> puff increases, allowing regenerative propagation of a Ca<sup>2+</sup> wave across the cell. In previous publications, we developed a stochastic model for IP<sub>3</sub>-evoked Ca<sup>2+</sup> signals in terms of the distributions of inter-puff intervals and puff durations (20, 21), which we use here to calculate the T<sub>av</sub> values entering the encoding relations in Fig. 3A in the same way as described in (20, 21). The distributions of both the inter-puff intervals and puff durations are generalized exponential functions (see eq. S1 with T<sub>min</sub> = 0 for this type of distribution). In the model, each cell has identical clusters of IP<sub>3</sub>Rs, the parameters that determine the distribution of puff durations are fixed, and the values of the parameters of the inter-puff interval distributions specify individual cells. The dependence of the inter-puff interval distribution parameters on IP<sub>3</sub> concentration was calculated from the DeYoung-Keizer model (21). The parameter ν (see eq. S1) consists of a constant and an additive part that depends on IP<sub>3</sub> concentration. Both have values typically in the range from 1.0 to ~4.0. We captured cell-to-cell variability by varying the constant part in a way that provided ν values from 1 to 3.85 at the first stimulation level. The range of values of T<sub>av1</sub> in Fig. 3A arises from this

cell-to-cell variability. Stimulation steps were modeled by increasing the IP<sub>3</sub> concentration from 0.5 μM by the steps specified in Fig. 3A. Average ISIs were calculated as the average first passage time for the transition from 0 to 4 open clusters. All other parameter values are given in (21).

### Statistical analysis of the encoding relation

The encoding relation (Eq. 3) predicts a linear relationship between individual T<sub>av1</sub> and T<sub>av2</sub> values. The linear fit was assessed in two ways. Pearson's correlation coefficient (ρ) measures how close data points are to a straight line, whereas the explained uncertainty (u<sub>ex</sub>) evaluates how much of the variance in the experimental data can be explained by fitting to a model like Eq. 3. In a regression model, it is generally true that

$$\sum (y_i - \bar{y})^2 = \sum (\hat{y}_i - \bar{y})^2 + \sum (y_i - \hat{y}_i)^2$$

with the mean  $\bar{y} = \frac{1}{N} \sum_{i=1}^N y_i$  and the predicted value  $\hat{y}_i = ax_i + b$ . The explained uncertainty  $u_{ex}$  is defined as the fraction of the total variance that remains if the regression error is subtracted (31):

$$u_{ex} = \frac{\sum (y_i - \bar{y})^2 - \sum (y_i - \hat{y}_i)^2}{\sum (y_i - \bar{y})^2} \quad (8)$$

The explained uncertainty thereby reports the extent to which a model adequately describes the experimental variation. For ρ and u<sub>ex</sub>, a value of 1 indicates a perfect linear correlation between values. We used both ρ and u<sub>ex</sub> to assess the linearity of the T<sub>av1</sub>-ΔT<sub>av</sub> relations for HEK293 cells and hepatocytes exposed to steps in stimulus concentration using our paired stimulus paradigm.

Our analysis of whether absolute responses (T<sub>av</sub>) or fold changes (β) provided the most reliable encoding of stimuli was performed for the fold change  $\beta = \Delta T_{av} / (T_{av1} - T_{min})$  (Eq. 3). The analysis is equally valid for the fold change of stochastic periods  $(T_{av2} - T_{min}) / (T_{av1} - T_{min})$ , which is equal to 1 - β (see Eq. 2). We compared the coefficients of variation CV(T<sub>pop2</sub>) and CV(β):

$$CV(T_{pop2}) = \frac{\sqrt{\frac{1}{N_{cell}-1} \sum_{j=1}^{N_{cell}} (T_{av2}^{(j)} - T_{pop2})^2}}{T_{pop2}} \quad (9)$$

T<sub>av2</sub><sup>(j)</sup> is the average ISI for an individual cell (j) responding to a second stimulus. T<sub>pop2</sub> is the average T<sub>av2</sub> from a population of N<sub>cell</sub> cells.

$$CV(\beta) = \frac{\sqrt{\frac{1}{N_{cell}-1} \sum_{j=1}^{N_{cell}} [(1-\beta)T_{av1}^{(j)} - T_{av2}^{(j)} + \beta T_{min}]^2}}{2 - 2\beta + \beta^2} \quad (10)$$

T<sub>av1</sub><sup>(j)</sup> and T<sub>av2</sub><sup>(j)</sup> are the average ISIs for an individual cell (j) responding to a first and second stimulus, respectively. T<sub>min</sub> is defined in Eq. 1. β is determined by  $\Delta T_{av} / (T_{av1} - T_{min})$  (see Eqs. 2 and 3). The expression in the numerator of Eq. 9 is the root mean square orthogonal distance of the data points from the line T<sub>av2</sub> = T<sub>pop2</sub>, and the numerator in Eq. 10 is the root mean square orthogonal distance of the data points from the line T<sub>av2</sub> = (1 - β)T<sub>av1</sub> + βT<sub>min</sub>.

In general, the integrated Ca<sup>2+</sup> signal comprises the integral over the initial transient and over the stationary part of the spike sequence. Because transients vary between cells and with stimulation conditions, no general statement about their integral is possible. For paired stimuli, the ratio of the integrated stationary signal approximately equals the ratio of Ca<sup>2+</sup> spike frequencies, because spike amplitudes were unaffected by stimulus intensity, and we did not detect any obvious change in spike duration. The IR of the stationary parts of the spike trains is therefore

$$IR = \frac{f_2}{f_1} = \frac{T_{av1}}{T_{av2}} = \frac{1}{1 - \beta \left(1 - \frac{T_{min}}{T_{av1}}\right)} \quad (11)$$

Mathematical descriptions of ISI distributions are provided in Supplementary Materials.

## SUPPLEMENTARY MATERIALS

www.sciencesignaling.org/cgi/content/full/7/331/ra59/DC1

Text S1. Mathematical description of ISI distributions.

Text S2. Mathematical derivation of the concentration-response relation.

Fig. S1. ISI distributions for hepatocytes.

Fig. S2.  $T_{av}$ - $\sigma$  relation.

Fig. S3. Responses of individual HEK293 cells to stimulation.

Table S1. Symbols and abbreviations.

Table S2. Selection of data for paired stimulation experiments.

## REFERENCES AND NOTES

- S. Tay, J. J. Hughey, T. K. Lee, T. Lipniacki, S. R. Quake, M. W. Covert, Single-cell NF- $\kappa$ B dynamics reveal digital activation and analogue information processing. *Nature* **466**, 267–271 (2010).
- M. Berridge, Inositol trisphosphate and calcium oscillations. *Biochem. Soc. Symp.* **74**, 1–7 (2007).
- A. B. Parekh, Decoding cytosolic Ca<sup>2+</sup> oscillations. *Trends Biochem. Sci.* **36**, 78–87 (2011).
- R. E. Dolmetsch, R. S. Lewis, C. C. Goodnow, J. I. Healy, Differential activation of transcription factors induced by Ca<sup>2+</sup> response amplitude and duration. *Nature* **386**, 855–858 (1997).
- G. Hajnóczky, L. D. Robb-Gaspers, M. B. Seitz, A. P. Thomas, Decoding of cytosolic calcium oscillations in the mitochondria. *Cell* **82**, 415–424 (1995).
- P. De Koninck, H. Schulman, Sensitivity of CaM kinase II to the frequency of Ca<sup>2+</sup> oscillations. *Science* **279**, 227–230 (1998).
- S. A. Walker, S. Kupzig, D. Bouyoucef, L. C. Davies, T. Tsuboi, T. G. Bivona, G. E. Cozior, P. J. Lockyer, A. Buckler, G. A. Rutter, M. J. Allen, M. R. Phillips, P. J. Cullen, Identification of a Ras GTPase-activating protein regulated by receptor-mediated Ca<sup>2+</sup> oscillations. *EMBO J.* **23**, 1749–1760 (2004).
- Q. Liu, S. A. Walker, D. Gao, J. A. Taylor, Y. F. Dai, R. S. Arkin, M. D. Bootman, H. L. Roderick, P. J. Cullen, P. J. Lockyer, CAPRI and RASAL impose different modes of information processing on Ras due to contrasting temporal filtering of Ca<sup>2+</sup>. *J. Cell Biol.* **170**, 183–190 (2005).
- J. K. Foskett, C. White, K. H. Cheung, D. O. D. Mak, Inositol trisphosphate receptor Ca<sup>2+</sup> release channels. *Physiol. Rev.* **87**, 593–658 (2007).
- J. S. Marchant, I. Parker, Role of elementary Ca<sup>2+</sup> puffs in generating repetitive Ca<sup>2+</sup> oscillations. *EMBO J.* **20**, 65–76 (2001).
- N. M. Woods, K. S. Cuthbertson, P. H. Cobbold, Repetitive transient rises in cytoplasmic free calcium in hormone-stimulated hepatocytes. *Nature* **319**, 600–602 (1986).
- T. Meyer, L. Stryer, Calcium spiking. *Annu. Rev. Biophys. Biophys. Chem.* **20**, 153–174 (1991).
- J. H. Levine, Y. Lin, M. B. Elowitz, Functional roles of pulsing in genetic circuits. *Science* **342**, 1193–1200 (2013).
- J. E. Purvis, G. Lahav, Encoding and decoding cellular information through signaling dynamics. *Cell* **152**, 945–956 (2013).
- A. Skupin, H. Kettenmann, U. Winkler, M. Wartenberg, H. Sauer, S. C. Tovey, C. W. Taylor, M. Falcke, How does intracellular Ca<sup>2+</sup> oscillate: By chance or by the clock? *Biophys. J.* **94**, 2404–2411 (2008).
- G. Dupont, L. Combettes, G. S. Bird, J. W. Putney, Calcium oscillations. *Cold Spring Harb. Perspect. Biol.* **3**, a004226 (2011).
- S. Dragoni, U. Laforenza, E. Bonetti, F. Lodola, C. Bottino, R. Berra-Romani, G. Carlo Bongio, M. P. Cinelli, G. Guerra, P. Pedrazzoli, V. Rosti, F. Tanzi, F. Moccia, Vascular endothelial growth factor stimulates endothelial colony forming cells proliferation and tubulogenesis by inducing oscillations in intracellular Ca<sup>2+</sup> concentration. *Stem Cells* **29**, 1898–1907 (2011).
- J. S. Altschuler, L. F. Wu, Cellular heterogeneity: Do differences make a difference? *Cell* **141**, 559–563 (2010).
- A. Skupin, M. Falcke, Statistical analysis of calcium oscillations. *Eur. Phys. J. Special Topics* **187**, 231–240 (2010).
- A. Skupin, M. Falcke, Statistical properties and information content of calcium oscillations. *Genome Inform.* **18**, 44–53 (2007).
- K. Thurley, M. Falcke, Derivation of Ca<sup>2+</sup> signals from puff properties reveals that pathway function is robust against cell variability but sensitive for control. *Proc. Natl. Acad. Sci. U.S.A.* **108**, 427–432 (2011).
- G. Moenke, M. Falcke, K. Thurley, Hierarchic stochastic modelling applied to intracellular Ca<sup>2+</sup> signals. *PLOS One* **7**, e51178 (2012).
- K. Thurley, I. F. Smith, S. C. Tovey, C. W. Taylor, I. Parker, M. Falcke, Timescales of IP<sub>3</sub>-evoked Ca<sup>2+</sup> spikes emerge from Ca<sup>2+</sup> puffs only at the cellular level. *Biophys. J.* **101**, 2638–2644 (2011).
- A. Skupin, H. Kettenmann, M. Falcke, Calcium signals driven by single channel noise. *PLOS Comput. Biol.* **6**, e1000870 (2010).
- R. F. Irvine, S. M. Lloyd-Burton, J. C. H. Yu, A. J. Letcher, M. J. Schell, The regulation and function of inositol 1,4,5-trisphosphate 3-kinases. *Adv. Enzyme Regul.* **46**, 314–323 (2006).
- S. C. Tovey, S. G. Dedos, E. J. A. Taylor, J. E. Church, C. W. Taylor, Selective coupling of type 6 adenylyl cyclase with type 2 IP<sub>3</sub> receptors mediates direct sensitization of IP<sub>3</sub> receptors by cAMP. *J. Cell Biol.* **183**, 297–311 (2008).
- J. E. Bleasdale, N. R. Thakur, R. S. Gremban, G. L. Bundy, F. A. Fitzpatrick, R. J. Smith, S. Bunting, Selective inhibition of receptor-coupled phospholipase C-dependent processes in human platelets and polymorphonuclear neutrophils. *J. Pharmacol. Exp. Ther.* **255**, 756–768 (1990).
- N. W. Seidler, I. Jona, M. Vegh, A. Martonosi, Cyclopiiazonic acid is a specific inhibitor of the Ca<sup>2+</sup>-ATPase of sarcoplasmic reticulum. *J. Biol. Chem.* **264**, 17816–17823 (1989).
- S. Dehaene, The neural basis of the Weber–Fechner law: A logarithmic mental number line. *Trends Cogn. Sci.* **7**, 145–147 (2003).
- S. C. Tippmann, R. Ivanek, D. Gaidatzis, A. Schöler, L. Hoerner, E. van Nimwegen, P. F. Stadler, M. B. Stadler, D. Schübeler, Chromatin measurements reveal contributions of synthesis and decay to steady-state mRNA levels. *Mol. Syst. Biol.* **8**, 593 (2012).
- T. A. Rooney, E. J. Sass, A. P. Thomas, Characterization of cytosolic calcium oscillations induced by phenylephrine and vasopressin in single fura-2-loaded hepatocytes. *J. Biol. Chem.* **264**, 17131–17141 (1989).
- P. E. Rapp, M. J. Berridge, The control of transepithelial potential oscillations in the salivary gland of *Calliphora erythrocephala*. *J. Exp. Biol.* **93**, 119–132 (1981).
- J. Garcia-Ojalvo, A. Martinez Arias, Towards a statistical mechanics of cell fate decisions. *Curr. Opin. Genet. Dev.* **22**, 619–626 (2012).
- A. Loewer, G. Lahav, We are all individuals: Causes and consequences of non-genetic heterogeneity in mammalian cells. *Curr. Opin. Genet. Dev.* **21**, 753–758 (2011).
- S. L. Spencer, S. Gaudet, J. G. Albeck, J. M. Burke, P. K. Sorger, Non-genetic origins of cell-to-cell variability in TRAIL-induced apoptosis. *Nature* **459**, 428–432 (2009).
- N. Barkai, B. Z. Shilo, Variability and robustness in biomolecular systems. *Mol. Cell* **28**, 755–760 (2007).
- P. Paszek, S. Ryan, L. Ashall, K. Sillitoe, C. V. Harper, D. G. Spiller, D. A. Rand, M. R. White, Population robustness arising from cellular heterogeneity. *Proc. Natl. Acad. Sci. U.S.A.* **107**, 11644–11649 (2010).
- S. Song, J. Li, L. Zhu, L. Cai, Q. Xu, C. Ling, Y. Su, Q. Hu, Irregular Ca<sup>2+</sup> oscillations regulate transcription via cumulative spike duration and spike amplitude. *J. Biol. Chem.* **287**, 40246–40255 (2012).
- C. Cohen-Saidon, A. A. Cohen, A. Sigal, Y. Liron, U. Alon, Dynamics and variability of ERK2 response to EGF in individual living cells. *Mol. Cell* **36**, 885–893 (2009).
- L. Goentoro, M. W. Kirschner, Evidence that fold-change, and not absolute level, of  $\beta$ -catenin dictates Wnt signaling. *Mol. Cell* **36**, 872–884 (2009).
- R. E. Lee, S. R. Walker, K. Savery, D. A. Frank, S. Gaudet, Fold change of nuclear NF- $\kappa$ B determines TNF-induced transcription in single cells. *Mol. Cell* **53**, 867–879 (2014).
- K. Aoki, Y. Kumagai, A. Sakurai, N. Komatsu, Y. Fujita, C. Shionyu, M. Matsuda, Stochastic ERK activation induced by noise and cell-to-cell propagation regulates cell density-dependent proliferation. *Mol. Cell* **52**, 529–540 (2013).
- I. Parker, J. Choi, Y. Yao, Elementary events of InsP<sub>3</sub>-induced Ca<sup>2+</sup> liberation in *Xenopus* oocytes: Hot spots, puffs and blips. *Cell Calcium* **20**, 105–121 (1996).

**Funding:** Supported by grants from the Wellcome Trust (101844) and Biotechnology and Biological Sciences Research Council (BB/H009736) to C.W.T., DFG (GRK 1772) to G.M., EMBO ASTF (Application Short-Term Fellowship) 398-09 to K.T., and Infusino Endowment to A.P.T. **Author contributions:** M.F., C.W.T., and A.S. designed the study. K.T., S.C.T., V.L.P., and A.M. collected experimental data and analyzed the data with C.W.T. and A.P.T. Mathematical analyses were performed by K.T., G.M., and A.S. and were supervised by M.F. The paper was written by C.W.T. and M.F. with input from all other authors. **Competing interests:** The authors declare that they have no competing interests.

Submitted 3 March 2014

Accepted 5 June 2014

Final Publication 24 June 2014

10.1126/scisignal.2005237

**Citation:** K. Thurley, S. C. Tovey, G. Moenke, V. L. Prince, A. Meena, A. P. Thomas, A. Skupin, C. W. Taylor, M. Falcke, Reliable encoding of stimulus intensities within random sequences of intracellular Ca<sup>2+</sup> spikes. *Sci. Signal.* **7**, ra59 (2014).

Supplementary Materials for  
**Reliable Encoding of Stimulus Intensities Within Random Sequences of  
Intracellular Ca<sup>2+</sup> Spikes**

Kevin Thurley, Stephen C. Tovey, Gregor Moenke, Victoria L. Prince, Abha Meena,  
Andrew P. Thomas, Alexander Skupin, Colin W. Taylor,\* Martin Falcke\*

\*Corresponding author. E-mail: martin.falcke@mdc-berlin.de (M.F.); cwt1000@cam.ac.uk (C.W.T.)

Published 24 June 2014, *Sci. Signal.* **7**, ra59 (2014)  
DOI: 10.1126/scisignal.2005237

**The PDF file includes:**

Text S1. Mathematical description of ISI distributions.

Text S2. Mathematical derivation of the concentration-response relation.

Fig. S1. ISI distributions for hepatocytes.

Fig. S2.  $T_{av}$ - $\sigma$  relation.

Fig. S3. Responses of individual HEK293 cells to stimulation.

Table S1. Symbols and abbreviations.

Table S2. Selection of data for paired stimulation experiments.

**Text S1: Mathematical description of ISI distributions**

Simple expressions for the ISI distributions for repetitive  $\text{Ca}^{2+}$  spikes have not yet been derived from mathematical models for  $\text{IP}_3\text{R}$  gating behavior. Hence, we work with equations describing the experimental data well but lacking the connection to single-channel models. We present two equations (eq. S1 and eq. S4), both of which fit the observed experimental distributions comparably well (22): Relaxation with rate  $\xi$  of the spike probability from 0 immediately after the refractory period to the probability per unit time  $\lambda$  (eq. S4), and a generalized exponential distribution with parameters  $\nu$  and  $\lambda$  (eq. S1). The generalized exponential distribution is known from radioactive decay, where it describes the distribution for the time of the decay of the last out of  $\nu$  atoms with a half-life  $\ln 2/\lambda$ . We cannot provide such a meaning of the parameters  $\nu$  and  $\lambda$  in terms of elements of the  $\text{Ca}^{2+}$  signaling pathway. The value of  $\nu$  can be directly determined from the value of  $\alpha$  (eq. S3). For vasopressin-stimulated hepatocytes, we obtain  $\nu = 500$ . This value is much too large to allow for an interpretation of  $\nu$  as the number of elementary  $\text{Ca}^{2+}$  release events from  $\text{IP}_3\text{R}$  channel clusters ( $\text{Ca}^{2+}$  puffs) between two cellular release spikes and  $\lambda$  as the average puff rate. Therefore, we consider  $\nu$  and  $\lambda$  merely as fit parameters. We use eq. S1, because it fits ISI distributions well (22) and it produces  $T_{\text{av}}-\sigma$  relations with the measured range of the slope  $\alpha$  between about 0.2 and 1.

$$\Lambda(t) = \begin{cases} 0, & t \leq T_{\min} \\ \lambda \nu \left(1 - e^{-\lambda(t-T_{\min})}\right)^{\nu-1} e^{-\lambda(t-T_{\min})}, & t > T_{\min} \end{cases} \quad (\text{S1})$$

$t$  denotes the time since the end of the last spike.  $T_{\min}$  is the sum of the spike duration and refractory period (Fig. 1C). The distribution has the average and variance:

$$\begin{aligned} T_{\text{av}} - T_{\min} &= \frac{1}{\lambda} [\Psi(\nu + 1) - \Psi(1)] \\ \sigma &= \frac{1}{\lambda} \sqrt{\Psi'(1) - \Psi'(\nu + 1)} + \sigma_{\min} \end{aligned} \quad (\text{S2})$$

$\Psi$  denotes the polygamma function and  $\Psi'$  its derivative. The coefficient of variation (CV) is defined by:

$$\text{CV} = \alpha = \frac{\sigma - \sigma_{\min}}{T_{\text{av}} - T_{\min}} = \frac{\sqrt{\Psi'(1) - \Psi'(\nu + 1)}}{\Psi(\nu + 1) - \Psi(1)} \quad (\text{S3})$$

and depends on  $\nu$  only. Note that the CV is equal to the slope  $\alpha$  of the the  $T_{\text{av}}-\sigma$  relation (Eq. 1). It can be used to determine the value of  $\nu$  that describes specific  $T_{\text{av}}-\sigma$  relations. The CV decreases with increasing  $\nu$ . In our analysis of ISI distributions,  $\nu$  describes the strength of negative feedback. We determined values of  $\nu$  for the experiments with hepatocytes stimulated with phenylephrine and vasopressin (fig. S1). We chose the value of  $\lambda$  to obtain values of  $T_{\text{av}}$  in the experimental range.

We use the relaxation equation (eq. S4) because it is descriptive, i.e. the parameters correspond to the rate of recovery from negative feedback ( $\xi$ ) and the spike probability after recovery ( $\lambda$ ). But eq. S4 is valid only for distributions with a slope of the  $T_{\text{av}}-\sigma$  relation greater than 0.63 (15). In the present study, the observed slopes for stimulated HEK293 cells and hepatocytes were all less than 0.4 (Fig. 1B, Fig. 2D, E, and fig. S3B).

$$\Lambda(t) = \begin{cases} 0, & t \leq T_{\min} \\ \lambda \left(1 - e^{-\xi(t-T_{\min})}\right) e^{-\int_0^{t-T_{\min}} \lambda(1-e^{-\xi\theta})d\theta}, & t > T_{\min} \end{cases}, \quad (\text{S4})$$

The dependence of the average ISI on  $\xi$  and  $\lambda$  following from eq. S4 is

$$T_{\text{av}} - T_{\min} = \frac{1}{\lambda} e^{\frac{\lambda}{\xi}} \left(\frac{\lambda}{\xi}\right)^{1-\frac{\lambda}{\xi}} \left[ \Gamma\left(\frac{\lambda}{\xi}\right) - \Gamma\left(\frac{\lambda}{\xi}, \frac{\lambda}{\xi}\right) \right] = \frac{1}{\lambda} F\left(\frac{\lambda}{\xi}\right) \quad (\text{S5})$$

The expression for the average ISI squared (second moment  $T^2$ ) of the stochastic part of the ISI  $T_{\text{av}} - T_{\min}$  and the standard deviation  $\sigma$  resulting from eq. S4 are

$$T^2 = \frac{2e^{\frac{\lambda}{\xi}}}{\lambda^2} {}_2F_2\left[\left[\left(\frac{\lambda}{\xi}, \frac{\lambda}{\xi}\right), \left(1 + \frac{\lambda}{\xi}, 1 + \frac{\lambda}{\xi}\right), -\frac{\lambda}{\xi}\right]\right]. \quad (\text{S6})$$

$$\sigma = \sqrt{T^2 - (T_{\text{av}} - T_{\min})^2} + \sigma_{\min}$$

$T_{\text{av}} - \sigma$  relations resulting from the above expressions for  $T_{\text{av}}$  (eq. S5) and  $\sigma$  (eq. S6) are shown in fig. S2.

### Text S2: Mathematical derivation of the concentration-response relation

Equation 2 implies, that  $\beta$  is 0 when  $\Delta[\text{CCh}]$  is 0. Hence, we can rewrite Eq. 2 first as a difference equation:

$$\begin{aligned} (T_{\text{av}}([\text{CCh}] + \Delta[\text{CCh}]) - T_{\min}) - (T_{\text{av}}([\text{CCh}]) - T_{\min}) &= -\beta([\text{CCh}], \Delta[\text{CCh}]) (T_{\text{av}}([\text{CCh}]) - T_{\min}) \\ &\approx -\frac{\partial\beta}{\partial\Delta[\text{CCh}]} \Delta[\text{CCh}] (T_{\text{av}}([\text{CCh}]) - T_{\min}) \end{aligned} \quad (\text{S7})$$

and in the limit  $\Delta[\text{CCh}] \rightarrow 0$  as a differential equation:

$$\frac{d(T_{\text{av}} - T_{\min})}{d[\text{CCh}]} = -\gamma (T_{\text{av}} - T_{\min}), \quad \gamma = \left. \frac{\partial\beta}{\partial\Delta[\text{CCh}]} \right|_{\Delta[\text{CCh}]=0} \quad (4)$$

In general,  $\beta$  could depend on the stimulation step and the initial Cch concentration as indicated in the difference equation, and then  $\gamma$  also depends on Cch concentration. That would not affect the validity of the differential equation, but it would affect its solution. The general solution of Eq. 4 is

$$T_{\text{av}} = e^{-\int_{[\text{CCh}]_{\text{ref}}}^{[\text{CCh}]} \gamma([\text{CCh}]) d[\text{CCh}]} (T_{\text{av,ref}} - T_{\min}) + T_{\min}. \quad (\text{S8})$$

For GPCR-stimulated  $\text{Ca}^{2+}$  spikes,  $\beta$  did not depend on the initial value. Thus,  $\gamma$  is constant, and the solution is an exponential dependence of  $T_{\text{av}}$  on  $\Delta[\text{CCh}] = [\text{CCh}] - [\text{CCh}]_{\text{ref}}$ :

$$T_{\text{av}} = e^{-\gamma([\text{CCh}] - [\text{CCh}]_{\text{ref}})} (T_{\text{av,ref}} - T_{\min}) + T_{\min} \quad (5)$$

Direct experimental confirmation of the differential equation (that is not through its mathematical solution) would require measurement of  $\beta$  for impractically small changes in carbachol concentration. Therefore, in addition to confirming Eq. 4 through its solution, we showed that the exponential dependence of  $\beta$  on steps in stimulation intensity was not restricted to small steps. Our derivation for the stimulus dependence of the fold change for large stimulation steps starts from the observation that  $\beta$  was independent of the starting value of the stimulation step and depended only on the step size (Fig. 3H) and the assumption that the spiking behavior of an individual cell to a specific stimulus is independent of previous exposures to the same stimulus. As an example, imagine an increase in stimulation from  $s_1$  to  $s_2$  to  $s_3$ . The assumption implies that an individual cell will have the value of the average ISI associated with  $s_3$  ( $T_{av3}$ ) whether the cell is directly exposed to  $s_3$  or exposed to  $s_3$  only after prior stimulation with  $s_1$  and  $s_2$ . The concentration steps are then  $\Delta s_{31}=s_3-s_1=s_3-s_2+s_2-s_1=\Delta s_{32}+\Delta s_{21}$ . The relationship between  $\beta$  and the difference in ligand concentration as shown in Fig. 3H indicated that the fold change is a function of the stimulation step:  $\beta(\Delta s_{ij})$ . The three stimulation steps cause the fold changes  $\beta(\Delta s_{31})$ ,  $\beta(\Delta s_{32})$ , and  $\beta(\Delta s_{21})$ . It follows from Eq. 3 that  $(1-\beta(\Delta s_{31}))=(1-\beta(\Delta s_{32}))(1-\beta(\Delta s_{21}))$ . The dependence of  $\beta$  on  $\Delta s$  can only comply with this equation, if  $1-\beta(\Delta s)=e^{-\gamma\Delta s}$  applies, that is

$$\beta(\Delta s) = 1 - e^{-\gamma\Delta s}.$$

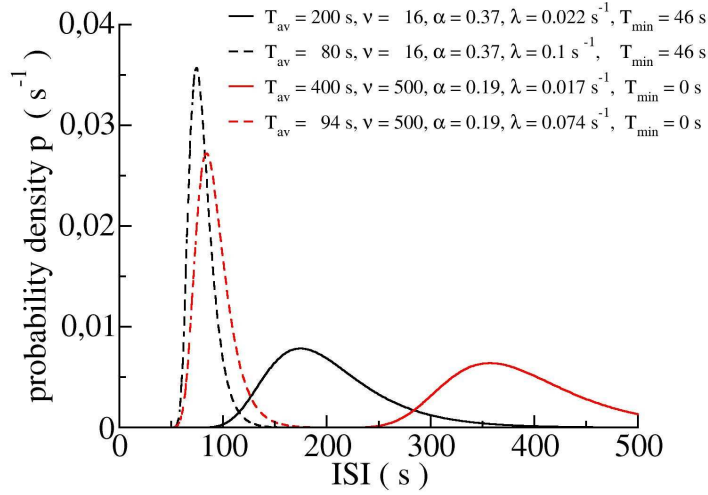


**Fig. S1. ISI distributions for hepatocytes.** The probability densities are calculated for hepatocytes stimulated with phenylephrine (black) or vasopressin (red) according to eq. S1. The values of  $v$  are obtained from the value of the slope of the  $T_{av}$ - $\sigma$  relation (eq. S3). We have chosen values of  $\lambda$  such that examples are plotted for small and large  $T_{av}$  like those observed experimentally for each agonist. The large values of  $v$  entail a refractory period even when  $T_{min} = 0$  s (red curves).

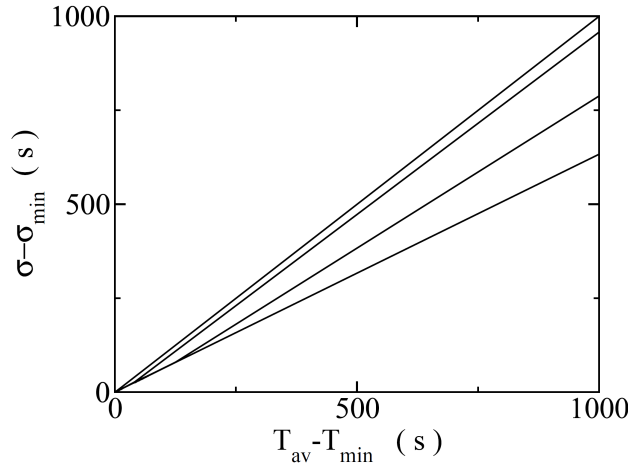


**Fig. S2.  $T_{av}$ - $\sigma$  relation.** The lines result from approximate expressions for  $T_{av}$  (eq. S5) and  $\sigma$  (eq. S6) and depend on  $\lambda$  and  $\xi$ . The value of  $\xi$  is kept constant along each line and  $\lambda$  varies from  $10^{-3} \text{ s}^{-1}$  to  $10 \text{ s}^{-1}$ . The values for  $\xi$  are with increasing slope  $10^{-5} \text{ s}^{-1}$ ,  $10^{-3} \text{ s}^{-1}$ ,  $10^{-2} \text{ s}^{-1}$ , and  $1 \text{ s}^{-1}$ .

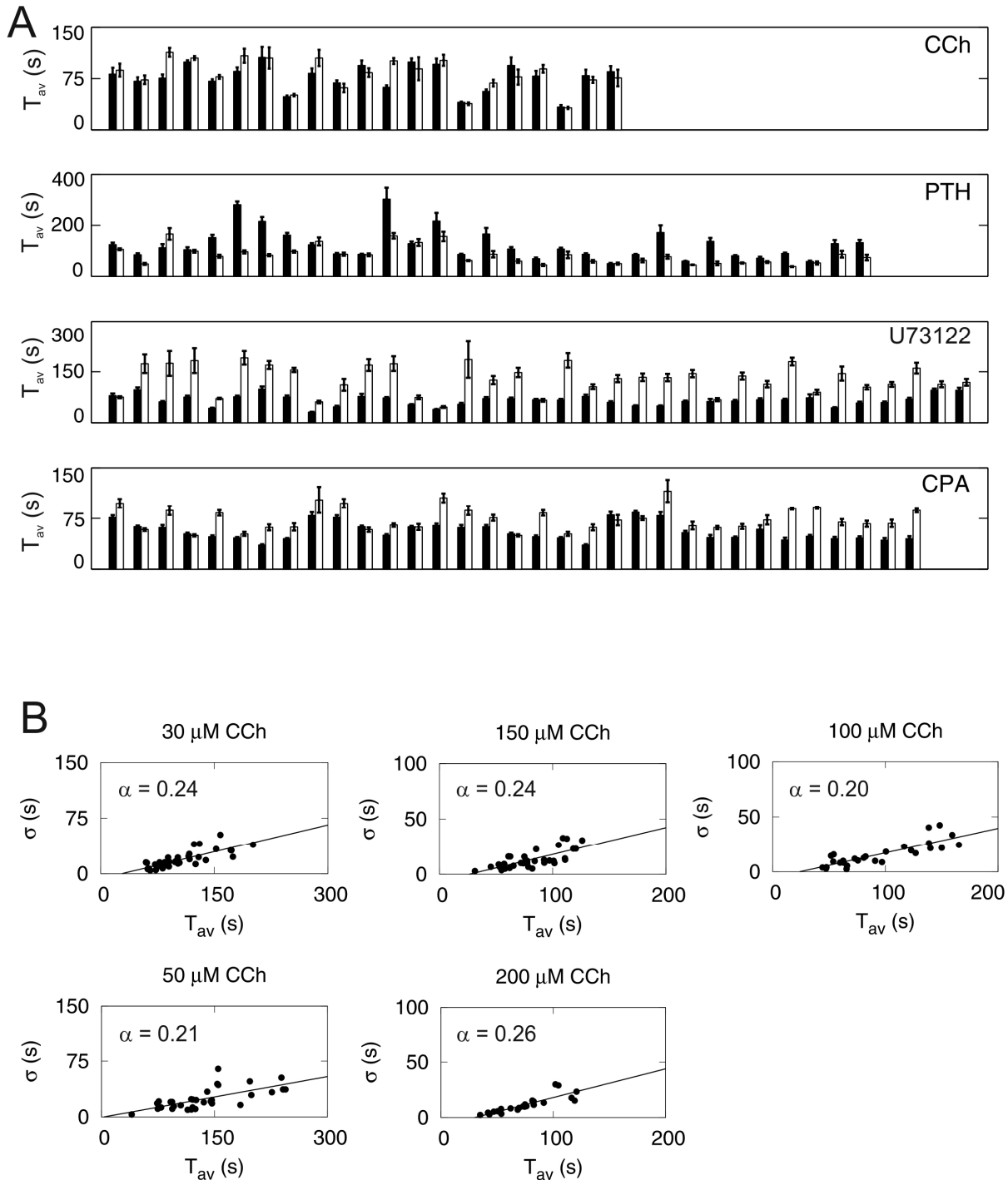


**Fig. S3. Responses of individual HEK293 cells to stimulation.** (A) HEK293 cells were stimulated first with 30  $\mu$ M carbachol (CCh) alone, and then with the same concentration of CCh in combination with a second stimulus (PTH 100 nM, U73122 100 nM, or CPA 10 nM). Each histogram pair shows  $T_{av} \pm$  SEM for the first ( $T_{av1}$ , black) and second ( $T_{av2}$ , white) period of stimulation for individual cells. For each cell, 7-33 spikes were analyzed for each condition. Summary data are presented in Fig. 2C. (B) Each point shows  $T_{av}$  and  $\sigma$  for a single cell stimulated as indicated. Cells in which fewer than 12 spikes were recorded were excluded from the analysis (the same criterion was applied to the data presented in Fig. 1B and 2D). The ratio of the axis scales is preserved between panels to allow direct comparison of slopes.

**Table S1. Symbols and abbreviations.**

Symbol	Description	Defining equation
$\alpha$	Slope of the $T_{av}$ - $\sigma$ relation. $\alpha^{-1}$ is the signal-to-noise ratio	Eq. 1, $\alpha^{-1} = \frac{T_{av} - T_{min}}{\sigma - \sigma_{min}}$
$\beta$	$\beta$ is the ratio $\Delta T_{av}/(T_{av1} - T_{min})$ and $1 - \beta$ is the fold-change of the average stochastic periods $(T_{av2} - T_{min})/(T_{av1} - T_{min})$ in a paired stimulation experiment	Eq. 2
<b>CCh</b>	Carbachol	
<b>CPA</b>	Cyclopiazonic acid. Reversible inhibitor of SERCA	
<b>CV</b>	Coefficient of variation, $CV = \text{standard deviation}/\text{average}$	
<b>CV(<math>T_{pop2}</math>)</b>	CV of $T_{av2}$	Eq. 9
<b>CV(<math>\beta</math>)</b>	Relative average root mean square distance of data points from $T_{av2} = (1 - \beta)T_{av1} + \beta T_{min}$	Eq. 10
$\Delta T_{av}$	Stimulation-dependent change of $T_{av}$ in a paired stimulation experiment	$\Delta T_{av} = T_{av1} - T_{av2}$
<b>ER</b>	Endoplasmic reticulum	
$\gamma$	Sensitivity of fold-changes to stimulation intensity, derivative of $\beta$ with respect to concentration step	Eq. 4
<b>IP<sub>3</sub></b>	Inositol 1,4,5-trisphosphate	
<b>IP<sub>3</sub>R</b>	IP <sub>3</sub> receptor	
<b>IR</b>	Ratio of integrated stationary $Ca^{2+}$ signals in a paired stimulation experiment	Eq. 11
<b>PLC</b>	Phospholipase C	
<b>PTH</b>	Parathyroid hormone	
$\rho$	Pearson's correlation coefficient	
<b>SERCA</b>	Sarco-endoplasmic reticulum $Ca^{2+}$ -ATPase	
$\sigma_{min}$	Standard deviation $\sigma$ of a ISI sequence with $T_{av} = T_{min}$	Eq. 1 and Fig. 1C
$T_{av}$	Average ISI of an individual cell	
$T_{av1(2)}$	Average ISI of an individual cell for the first (second) stimulus in a paired stimulation experiment	
$T_{av,ref}$	The average ISI of an individual cell measured for a reference stimulus concentration	Eq. 5
$T_{min}$	Sum of spike duration and refractory period, minimal $T_{av}$ of a cell population	Eq. 1 and Fig. 1C
$T_{pop}$	Population average of $T_{av}$	Eq. 7
$T_{pop2}$	Population average of $T_{av2}$	
$T_{pop,ref}$	The population average $T_{pop}$ for a reference stimulus concentration	Eq. 7
$u_{ex}$	Explained uncertainty. Fraction of the total variance that remains when the regression error has been subtracted	Eq. 8

**Table S2. Selection of data for paired stimulation experiments.** The table shows the number of cells selected for the final analysis from all those examined using the criteria defined in Materials and Methods. The total number of cells analyzed (all live cells detected in the fields examined) and the number of cells producing repetitive  $\text{Ca}^{2+}$  spikes in response to only the first, only the second, or both stimuli, is provided. The last columns show the numbers of cells that continued to spike in response to both stimuli and for which at least 7 stationary ISIs were resolved during the recording period.

Stimulus step CCh ( $\mu\text{M}$ )	Number of cells	Number of cells exhibiting $\text{Ca}^{2+}$ spikes			Cells with at least 7 stationary ISI for both stimuli		
		1 <sup>st</sup> only	2 <sup>nd</sup> only	Both	Number of cells	% of all cells	% of cells with spikes
30 to 100	178	0	36	74	21	12	28
30 to 150	227	0	69	93	25	11	27
30 to 200	198	1	65	66	17	9	26
50 to 100	249	4	33	109	18	7	17
50 to 150	125	2	30	42	19	15	45
50 to 200	148	1	42	31	10	7	32